Pressure dependence of the magnetic structure of the itinerant electron magnet MnSi

2005 J. Phys.: Condens. Matter 17 1635

(http://iopscience.iop.org/0953-8984/17/10/018)

INSTITUTE OF PHYSICS PUBLISHING JOURNAL OF PHYSICS: CONDENSED MATTER

J. Phys.: Condens. Matter **17** (2005) 1635–1644 doi:10.1088/0953-8984/17/10/018

Pressure dependence of the magnetic structure of the itinerant electron magnet MnSi

B Fåk[1], R A Sadykov[2], J Flouquet[1] and G Lapertot[1]

[1] Commissariat à l'Energie Atomique, Département de Recherche Fondamentale sur la Matière Condensée, SPSMS, 38054 Grenoble, France
[2] Institute for High-Pressure Physics, Russian Academy of Sciences, 142190 Troitsk, Moscow region, Russia

Received 17 December 2004, in final form 3 February 2005
Published 25 February 2005
Online at stacks.iop.org/JPhysCM/17/1635

Abstract

Elastic neutron scattering measurements have been performed under hydrostatic pressure on single-crystalline MnSi. The scaling between the staggered moment and the transition temperature of the helical magnetic structure does not follow predictions from spin-fluctuation theories. For pressures below $p^* \approx 12$–13 kbar, where the transition is second order, the length of the helix decreases with increasing temperature. Such a behaviour is not expected for a ferromagnetic Dzyaloshinsky–Moriya instability. With increasing pressure, the length of the helix also decreases, but there is a lock-in to an incommensurate temperature-independent value above p^*, where the phase transition is first order.

(Some figures in this article are in colour only in the electronic version)

1. Introduction

MnSi is a weakly ferromagnetic itinerant 3d-electron metal that crystallizes in the non-centrosymmetric cubic space group $P2_13$. The lack of inversion symmetry leads to an antisymmetric Dzyaloshinsky–Moriya (DM) interaction term $D\mathbf{k} \cdot (\mathbf{S}_1 \times \mathbf{S}_2)$ originating in the spin–orbit coupling [1–4]. As a consequence, a long-wavelength (∼180 Å) helical spin-density wave (SDW) is formed below $T_C = 29.5$ K [5]. Weak crystal-field anisotropies fix the propagation vector $\mathbf{k}$ to the cubic [111] axis (in zero magnetic field). The propagation vector is $\mathbf{k} = (\delta, \delta, \delta)$, with $\delta \approx 0.015$ rlu at zero pressure and temperature. The ordered magnetic moment $\mathbf{M}$ is perpendicular to $\mathbf{k}$, and its low-T magnitude of 0.4 μ_B is much smaller than the high-T effective moment. The chirality of the magnetic structure is single-handed, as determined from polarized neutron scattering [6–8].

With increasing pressure, the magnetic transition temperature decreases and the magnetic order finally disappears at a critical pressure of $p_c = 14.7 \pm 0.1$ kbar in transport measurements [9–11]. Below $p^* \approx 12$–13 kbar, the transition is second order, while above p^*,

Table 1. Experimental conditions. F_a is the applied force at room temperature and p_a the corresponding nominal pressure; p_{obs} is the pressure at low temperatures obtained from the magnetic transition temperature T_C. The material used for the holder is also given.

F_a (10^4 N)	p_a(300 K) (kbar)	p_{obs}(2 K) (kbar)	T_C (K)	Holder
0	0	0	29.24 (5)	Teflon
2.2	12.3	6.6	19.59 (2)	Teflon
2.9	16.2	11.2	12.14 (6)	Teflon
3.3	18.5	12.0	10.55 (2)	Teflon
3.9	21.8	13.2	7.89 (1)	Teflon
4.5	25.2	14.2	3.59 (2)	Teflon
3.3	18.5	13.1	7.95 (3)	Pb

it is weakly first order [12]. Close to the quantum phase transition (QPT) at p_c, the temperature-dependent part of the electrical resistivity shows deviations from Fermi liquid behaviour, with $\Delta\rho = AT^{3/2}$ over a wide temperature range [10, 13–16].

NMR measurements suggest that the standard scaling relation, obtained in spin-fluctuation theories [17], between the transition temperature T_c and the magnitude of the ordered moment M as a function of pressure,

$$T_c(p) \propto M^{\alpha}(p) \tag{1}$$

with $\alpha = 3/2$, is not observed [18, 19]. The aim of the present work was to use a more direct method, neutron elastic scattering investigation, to measure the sublattice magnetization of a high-quality single crystal of MnSi under hydrostatic pressure, and to verify the scaling relation, equation (1), for pressures up to p_c.

2. Experimental aspects

2.1. Sample and sample environment

High-quality single crystals were pulled from a stoichiometric melt of high-purity (>99.995%) elements, using radio-frequency heating and a cold copper crucible. The manganese was acid etched before the synthesis. An x-ray powder diffraction study was performed on the polycrystalline sample before the growth and Laue diffraction on the pulled crystal. Scanning electron microscope microanalysis and backscattered electron images were used to study the phase purity. None of those characterizations revealed deviations from known crystallographic parameters or the presence of other metallurgical phases. The mosaicity of the samples, which were not annealed, was 0.2°. A crystal was cut using electroerosion into a cylinder of diameter 4 mm and height 7 mm, with the $[1\bar{1}0]$ axis along the cylinder axis, which was mounted vertical.

One of the main problems with measurements of MnSi under pressure is its extreme sensitivity to deviations from hydrostatic conditions, which are always present in clamp cells. In order to improve the hydrostaticity, the sample was not glued to any support but suspended in the liquid pressure transmitter consisting of a 50–50% mixture of FC75/FC84 Fluorinert inside a Teflon or lead holder of inner diameter 4.4 mm. The holder was mounted in a Ni–Cr–Al clamp cell from Troitsk, with the inner (outer) diameter of 4.7 (12.7) mm. Ni–Cr–Al pistons were used, except at the highest pressure where non-magnetic tungsten carbide pistons were used. Details are given in table 1. A magnetic field in the horizontal scattering plane was used to induce a *controlled* magnetic domain population in the sample, which is particularly

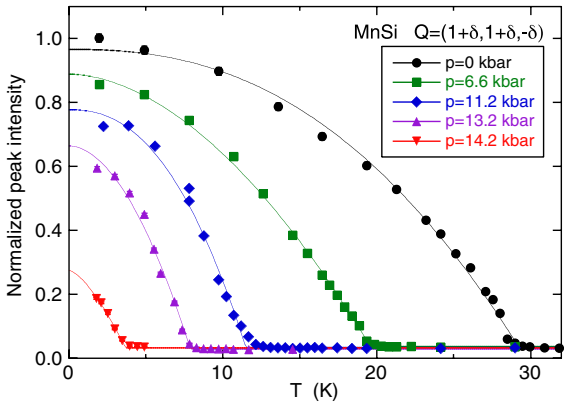

Figure 1. Temperature dependence of the peak height of the magnetic satellite at $\mathbf{Q} = (110)+\mathbf{k}_2 = (1+\delta, 1+\delta, -\delta)$ and $H = 0.1$ T for different pressures p, normalized to the nuclear Bragg peak intensity. The curves are guides to the eye.

important at high pressures. The crystallographic $[11\bar{1}]$ axis was parallel to the magnetic field with high precision, better than 0.2°.

Traditionally, the magnetic structure of MnSi has been studied by means of small-angle neutron scattering, due to the smallness of the magnetic propagation vector $|\mathbf{k}|$. However, the high background from pressure cells in the forward direction makes this technique unfavourable. We therefore chose to study the magnetic structure close to the (110) nuclear Bragg peak, using the IN12 cold-neutron triple-axis spectrometer at the high-flux reactor of the Institut Laue-Langevin (Grenoble, France), operated in a W configuration with a vertically focusing PG(002) monochromator. A flat PG(002) analyser set at elastic energy transfer was used to reduce the background. A liquid nitrogen cooled Be filter was used in the incident beam to suppress second-order contamination. The required Q resolution was obtained by using tight collimation (20′ throughout) and cold neutrons. The neutron wavevector $k_i = 1.38$ Å^{-1} was chosen so that the incident and scattered beam did not hit the pillars of the magnet, still allowing the field to be along the $[11\bar{1}]$ direction. The (110) nuclear Bragg peak was then observed at a scattering angle of 90°.

2.2. *Pressure determination*

The use of a triple-axis spectrometer and a horizontal magnet with limited angular access precluded the use of standard methods for determining the pressure in neutron scattering experiments, such as measuring the lattice parameter of a NaCl crystal. Instead, we determined the transition temperature T_C for the magnetic order and used the pressure dependence $T_C(p)$ known from the literature [18] to determine the pressure p. The thermalization time constant of the sample was carefully determined by monitoring the magnetic Bragg peak intensity after a temperature change in a region where the moment varies rapidly with T. Due to the small size of the pressure cell used, the thermalization of the sample was reached within 15 min in the actual temperature range. All measurements of $M(T)$ were made by increasing the temperature; no search for hysteresis was made.

Examples of the temperature dependence of the magnetic peak intensity, $I_M(T) \propto M^2(T) + B$, where B is the background from the pressure cell and the tail of the nuclear Bragg peak at (110), are shown in figure 1. From these data, $T_C(p)$ and hence p could be

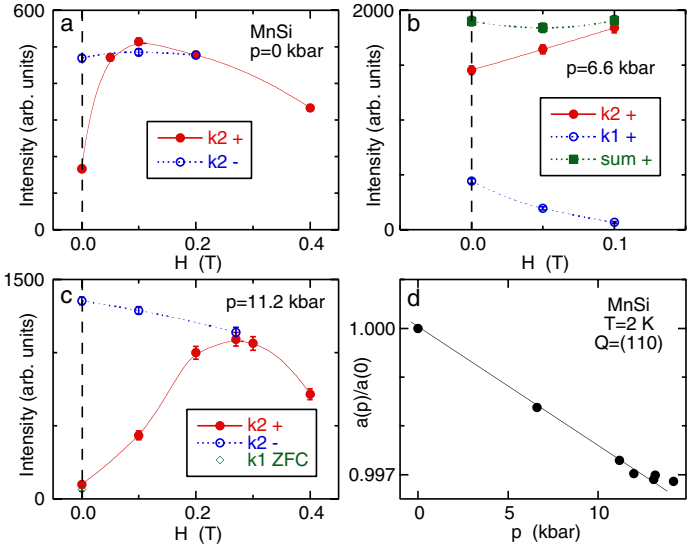

Figure 2. ((a)–(c)) Field dependence of the magnetic Bragg peak intensity at $T = 2$ K for a magnetic field applied along the $[11\bar{1}]$ direction, i.e. along $\mathbf{k}_2$. (a) $p = 0$ kbar, domain $\mathbf{k}_2$ for increasing (+) and decreasing (−) field. (b) $p = 6.6$ kbar, domains $\mathbf{k}_1$ and $\mathbf{k}_2$ and their sum for increasing (+) field. (c) $p = 11.2$ kbar, domain $\mathbf{k}_2$ for increasing (+) and decreasing (−) field, and domain $\mathbf{k}_1$ for zero-field cooling. (d) Pressure dependence of the low-temperature lattice parameter $a(p)$ normalized to $a(0)$. Symbols are experimental data and lines are guides to the eye.

accurately determined. The corresponding values are given in table 1. The difference between the applied and the measured pressure is partly due to the freezing of the pressure transmitter, estimated to 2–2.5 kbar (the cell was slowly cooled to minimize the formation of pressure gradients), and partly due to friction losses in the pressure cell. The latter is approximately $25 \pm 7\%$ of the applied pressure, a value typical for this kind of cell.

The lattice parameter of MnSi as a function of pressure, $a(p)$, determined from longitudinal scans of the (110) nuclear Bragg peak, is shown in figure 2(d). The use of a triple-axis spectrometer does not allow a precise determination of the absolute value of the lattice parameter ($a \approx 4.558$ Å at zero pressure), but the relative pressure dependence can be determined accurately taken appropriate precautions for the centring of the crystal. For $p < 13$ kbar, the linear pressure dependence confirms the pressure determination based on the $T_C(p)$ discussed above. The change in slope at 13 kbar could be related to the transition becoming first order. This would give a value of p^* of 13 kbar, in fair agreement with values quoted in the literature [10, 11].

2.3. Domain population

The magnetic moment at a position $\mathbf{r}$ along a helix can be expressed as

$$\mathbf{M}(\mathbf{r}) = M[\hat{\mathbf{u}}\cos(\mathbf{k}\cdot\mathbf{r}) + \hat{\mathbf{v}}\sin(\mathbf{k}\cdot\mathbf{r})], \tag{2}$$

where $\hat{\mathbf{u}}$ and $\hat{\mathbf{v}}$ are two orthogonal unit vectors perpendicular to $\mathbf{k}$. In MnSi, where $\mathbf{k}$ is along a threefold axis of the cubic structure, there are four equivalent magnetic propagation vectors, $\mathbf{k}_1 = (\delta, \delta, \delta)$, $\mathbf{k}_2 = (\delta, \delta, -\delta)$, $\mathbf{k}_3 = (\delta, -\delta, \delta)$, and $\mathbf{k}_4 = (\delta, -\delta, -\delta)$, each corresponding to a so-called K domain. Because of the lack of inversion symmetry, the chirality is single handed, and the same helix is observed at $+\mathbf{k}$ and $-\mathbf{k}$ (there are thus no chiral domains).

With unpolarized neutrons, there are thus eight magnetic satellite peaks around each nuclear Bragg peak, corresponding to $\pm\mathbf{k}_j$ with $j = 1, \ldots, 4$. For an unstrained sample, one would expect to see equal populations of the four K domains. This is observed experimentally for our sample. However, the application of pressure may induce an unequal domain population, due to deviations from hydrostaticity. This effect is particularly severe in MnSi. We note in passing that strong deviations from hydrostaticity in some pressure cells (not used in this work) may even change the direction of the propagation vector. In order to determine the sublattice magnetization under pressure, one would thus need to measure all four domains. Since only two of the four domains are observable in a given scattering plane, this poses problems in neutron scattering experiments. We therefore used a magnetic field parallel to the crystallographic $[11\bar{1}]$ axis to favour the population of the $\mathbf{k}_2$ domain.

The application of a magnetic field H has three effects in MnSi, in order of increasing field: domain repopulation, canting of the moment, and reorientation of the propagation vector parallel to H [5]. The field applied in the present work is too weak to induce the third effect. Figures 2(a)–(c) show the domain repopulation with increasing field in a zero-field cooled state: the intensity increases initially in the $\mathbf{k}_2$ domain and decreases in the $\mathbf{k}_1$ domain. At higher fields, the intensity decreases due to the canting of the moments. As the field is decreased again, the intensity increases as the canting disappears, while the domain population remains unchanged. At higher pressures, a higher field is required to populate the $\mathbf{k}_2$ domain, since the pressure gradients compete with the effect of the field. Also, the $\mathbf{k}_2$ domain has a tendency to depopulate at zero field as a function of time, and hence most measurements were done at a field of 0.1 T. This maintains the domain population while the effect of canting on the observed intensity is negligible. By tilting the cryostat, it was possible to verify that the population of the out-of-plane domains $\mathbf{k}_3$ and $\mathbf{k}_4$ vanished along with $\mathbf{k}_1$ in an applied field along the $[11\bar{1}]$ direction. We also found that the intensity of the satellite peak at $\mathbf{k}_2$ was always equal to that at $-\mathbf{k}_2$, as expected for unpolarized neutrons, since the same domain is observed at $\pm\mathbf{k}_2$ for a single-handed helix.

2.4. Methodology

In order to determine the sublattice magnetization, scans through the magnetic satellite peaks were made at different temperatures and pressures. Transverse scans, i.e. scans with the scan direction perpendicular to the wavevector $\mathbf{Q} = \boldsymbol{\tau} + \mathbf{k}_2$, have the advantage of not being contaminated by the nearby nuclear Bragg peak at $\boldsymbol{\tau} = (110)$. Longitudinal scans, on the other hand, are necessary for determining the pressure and temperature dependence of the length (or δ) of the propagation vector. The tail of the nuclear Bragg peak was straightforwardly removed from these scans, either by taking off a sloping background or by subtracting the same scans taken above the transition temperature. Longitudinal and transverse scans give the same results for the magnitude of the moment and we use the average of the two scan types to improve the quality of the data. Examples of scans are shown in figure 3. No broadening of the magnetic satellite peaks was observed within the instrumental resolution, i.e. the magnetic order remains long range at all T and p. Within the experimental precision, the propagation vector $\mathbf{k}_2 = (\delta_x, \delta_y, -\delta_z)$ does not turn with pressure or temperature, i.e. $\delta_x = \delta_y = \delta_z = \delta$. Only the magnitude of δ changes with temperature or pressure. The intensity of the magnetic scattering was normalized to the integrated intensity of scans of the nuclear Bragg peak at (110). Due to the small compressibility of MnSi (see figure 2(d)), we assume that the magnetic form factor does not vary significantly with pressure at the Q value studied. The statistical errors (shown in the figures) are smaller than errors in the normalization (due to inaccuracies in the crystal alignment) and in the pressure determination.

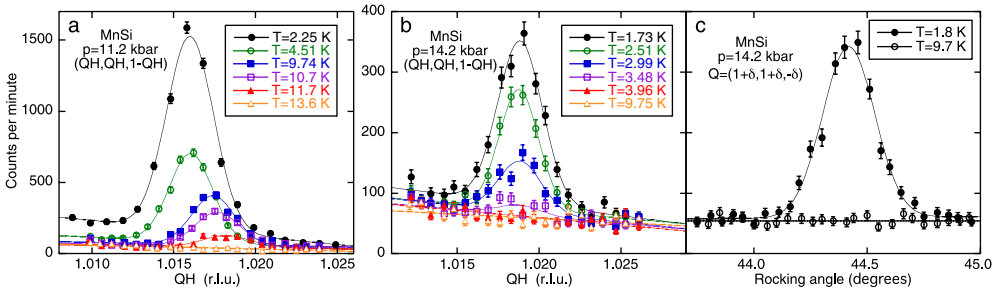

Figure 3. ((a), (b)) Longitudinal scans of the $\mathbf{k}_2$ domain at different temperatures and $H = 0.1$ T. Note that the peak position depends on temperature for $p < p^*$ (a) while it is constant for $p > p^*$ (b). (c) Transverse scans of the $\mathbf{k}_2$ domain above p^* for temperatures below and above T_C, at $H = 0.1$ T. The lines are fits to a Gaussian plus a sloping background.

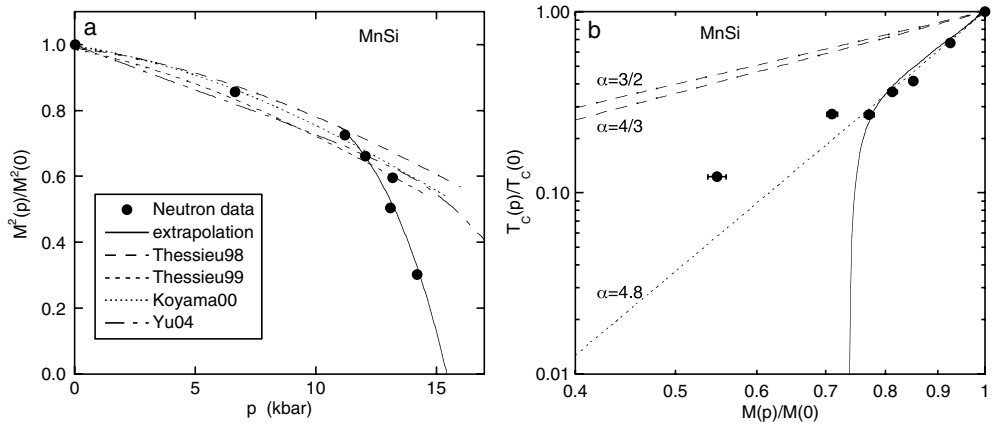

Figure 4. (a) Pressure dependence of the intensity $I_M \propto M^2(p)$ (symbols) of the magnetic satellite peaks of MnSi at $T = 2$ K and $H = 0.1$ T, normalized to the zero-pressure value. The extrapolation to zero intensity is shown by the solid curve. The broken curves show the magnetization squared, M^2, obtained from the NMR frequency by Thessieu *et al* [18, 19] and Yu *et al* [21] as well as the bulk magnetization measurements of Koyama *et al* [20]. (b) Scaling behaviour (on a double-logarithmic scale) of the reduced transition temperature $T_C(p)/T_C(0)$ with respect to the reduced ordered magnetic moment $M(p)/M(0)$ with pressure as an implicit parameter. Symbols are neutron data. The solid curve shows NMR data [19], the dashed lines show the spin-fluctuation-theory prediction for an itinerant ferromagnet (antiferromagnet) with $\alpha = 3/2$ ($\alpha = 4/3$) in equation (1), and the dotted line is a fit of equation (1) yielding $\alpha \approx 4.8$.

3. Results

3.1. Moment magnitude

The pressure dependence of the magnetic intensity ($\propto M^2$) at $H = 0.1$ T and extrapolated to zero temperature is shown in figure 4(a). The data are in good agreement with $M^2(p)$ extracted from magnetization and NMR measurements [18–21] up to $p^* \approx 12$–13 kbar and also with μSR measurements under pressure [22]. Above p^*, our direct measurements of the staggered magnetization M using neutron scattering show a substantially reduced moment. Although there is some ambiguity as regards how to extrapolate the moment to zero temperature at the highest pressure, $p = 14.2$ kbar, chiefly since the lowest temperature measured is quite close to T_C, it is nevertheless clear that the moment is reduced above p^*. The 'missing' moment

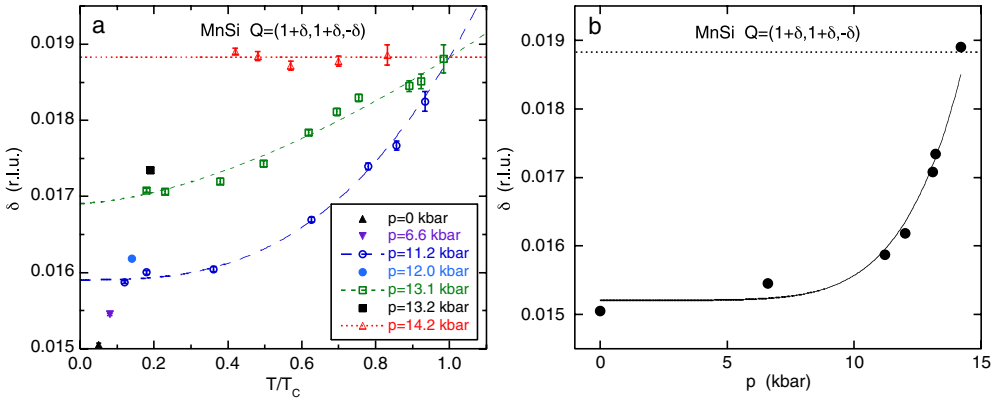

Figure 5. (a) Temperature dependence (in reduced units) of δ (∼inverse length) of the helix at different pressures, at $H = 0.1$ T. (b) Pressure dependence of δ at the lowest temperature measured, $T = 1.5$ K, and $H = 0.1$ T. The lines are guides to the eye.

might either be located at other points in the Brillouin zone (see e.g. [16] for the situation above p_c) or be dynamic in origin. Inhomogeneity is an alternative explanation, which is discussed in section 4. We did not perform any measurements above p_c. The extrapolated critical pressure is $p_c = 15.4$ (2) kbar, in fair agreement with $p_c = 14.7$ (1) kbar from macroscopic measurements [10, 11].

Figure 4(b) shows the reduced transition temperature $T_C(p)/T_C(p=0)$ as a function of the reduced magnetic moment $M(p)/M(p=0)$ extrapolated to zero temperature. Pressure is here an implicit variable, which has the advantage that possible errors in the pressure determination play no role. The data clearly do not fulfil the simple scaling relation equation (1) with $\alpha = 3/2$, expected for a weak itinerant ferromagnet [17]. For pressures below p^*, i.e. all points except those with $M(p)/M(0)$ less than 0.6, a coefficient $\alpha \approx 4.8$ is found, far beyond any expected value (for weakly antiferromagnetic itinerant systems, one expects $\alpha \approx 4/3$ [23]). The magnetization and NMR data of Thessieu *et al* [18, 19] are (again) in good agreement with ours for $p < p^*$, but not above.

3.2. Length of the helix

For a propagation vector $\mathbf{k} = (\delta, \delta, \delta)$, the length of the helix is $1/\delta$ (in units of interplanar distances along the [111] direction). The low-temperature value of δ clearly increases with pressure, as shown in figure 5(b). It goes from $\delta = 0.015\,05$ (2) rlu at zero pressure to $\delta = 0.018\,91$ (4) rlu at $p = 14.2$ kbar. This means that the system becomes less ferromagnetic (shorter length of the helix) with increasing pressure.

Below p^*, where the transition is second order, δ increases with temperature (see figure 5(a)). Although it is difficult to measure δ with precision very close to the transition temperature T_C (due to the weak magnetic intensity), there is no sign that δ diverges at T_C. Instead, it seems that the second-order transition occurs exactly when δ reaches the 'magical' value of 0.018 91 rlu (see figure 5(a)). Above p^*, where the transition is first order, δ is temperature independent. Hence, the change from a second-to a first-order transition is accompanied by a lock-in of the propagation vector. It thus seems that MnSi cannot support a helical structure with δ longer than 0.018 91 rlu, either as a function of pressure or as a function of temperature. This is one of the major and most puzzling findings in this work.

4. Discussion

The present work was motivated by the ^{29}Si NMR measurements of Thessieu *et al* [18, 19], which suggested that (i) the scaling relation of equation (1) was not fulfilled and (ii) the NMR signal persisted, albeit substantially broadened, above the critical pressure p_c. ^{29}Si NMR measurements probe the local magnetic field at the Si site induced by the spin polarization of the Mn 3d electrons. Although the local magnetization inferred from NMR data has the same pressure dependence as the saturated magnetic moment from bulk magnetization measurements [18, 19], it is still important to verify these results by a more direct measurement of the sublattice magnetization, such as a neutron scattering one. Our neutron data confirms the violation of the scaling relation of equation (1); see figure 4. Figure 4(a) shows that the magnetic intensity extrapolates to zero close to p_c, which would imply the absence of long-range magnetic order above p_c. This, at first, seems in contradiction with the NMR data. A possible explanation is that the NMR signal above p_c is related to short-range correlations or 'local order' observed by means of neutron scattering above p_c [16]. Indeed, the NMR signal observed above p_c is substantially broadened, which could be expected for short-range correlations. More recent ^{29}Si NMR measurements by Yu *et al* [21] also show a broadened resonance signal above p_c, in qualitative agreement with earlier work [18, 19]. In addition, they found a sudden decrease of the total spectral intensity at $p > p^*$, which was interpreted as due to an inhomogeneous magnetic phase. Since the transition above p^* is first order, internal strains in the small-grained powder sample used or slightly non-hydrostatic pressure conditions can easily give rise to such inhomogeneities due to phase separation. This effect, if present in our single-crystalline sample, could explain the sudden drop we observe in the magnetic intensity near p^* (cf figure 4(a)), since the neutron intensity is proportional to the product of the ordered moment squared and the volume of the part of the sample contributing to the magnetic intensity.

In addition to well-defined magnetic Bragg peaks below p_c at satellite positions of type $\mathbf{k} = (\delta, \delta, \delta)$, Pfleiderer *et al* [16] also observed broad features above p_c at positions corresponding to another wavevector, $\boldsymbol{\kappa} = (\epsilon, \epsilon, 0)$, where ϵ is of the same order as δ. This is the same position as where the critical scattering at zero pressure is maximal [24]. In our measurements, we did not investigate this position. However, no broad features were observed at (δ, δ, δ)-type positions. In fact, the magnetic Bragg peaks at $\mathbf{k} = (\delta, \delta, \delta)$ are sharp all the way up to $T_c(p)$ at all pressures $p < p_c$. The non-observation of diffuse scattering above the transition temperature could be related to the lower sensitivity in our measurements due to higher background from the pressure cell. In fact, ring-like diffuse scattering resembling the features observed by Pfleiderer *et al* [16] has been observed at zero pressure near the transition temperature [25].

The crossover from a second-order to a weakly first-order transition observed in magnetic susceptibility measurements at a pressure of $p^* = 12$–13 kbar can be understood in the context of non-critical soft modes characteristic of an itinerant electron system at low temperature. In fact, the phase transition for both a weak itinerant ferromagnet and a weak itinerant helimagnet can be shown theoretically to become first order if the transition temperature is low enough [26, 27]. In MnSi, this crossover does indeed occur at low temperatures: $T_C \approx 12$ K at p^*. Renormalization group theory also predicts a first-order transition in MnSi [1]. In our measurements, a strong decrease in the ordered magnetic moment is observed at p^*, which is consistent with a change from second to first order. However, the temperature dependence of the moment (see figure 1) is the same below and above p^* within the experimental precision.

Theoretically, the inverse length of the helix, δ, is determined by a balance between the ferromagnetic interaction and the DM interaction, $D\mathbf{k}\cdot(\mathbf{S}_1 \times \mathbf{S}_2)$ [1–4]. We find experimentally

that δ depends on temperature below p^*. This is unexpected, since the strength of the DM interaction term, D, is temperature independent. Since MnSi is an itinerant magnet, the most likely scenario is that the spin fluctuations modify the ferromagnetic coupling and in that way introduce a temperature-dependent δ. However, it is difficult to understand in a spin-fluctuation scenario how δ could become temperature independent above p^*, where the phase transition is first order. The length of the helix at low temperatures decreases from $1/\delta = 66.4$ (0.1) to 52.9(1) interplanar distances along the [111] axis as the pressure goes from 0 to 14.2 kbar. While the accuracy in the determination of the length of the helix is not sufficient to allow us to reach a conclusion on whether the 'lock-in' value is strictly commensurate or incommensurate, it is energetically rather insignificant whether the helix is 52 or 53 interplanar distances long. This can also be seen from the pitch angle of 6.8°, which does not correspond to any particular symmetry of the crystal. In any case, the incommensurate to commensurate transition expected in general for helical structures should not occur in MnSi, since the absence of inversion symmetry prevents the occurrence of a Lifshitz point [28].

In conclusion, our neutron scattering study of the helimagnetic structure of MnSi under highly hydrostatic pressure conditions shows that the scaling between the sublattice magnetization and the transition temperature does not follow predictions from spin-fluctuation theories. We also find that the length of the helix is temperature dependent below p^*, in qualitative agreement with zero-pressure work [25], but locks in at a temperature-independent, probably incommensurate, value above p^*. The temperature and pressure dependence of the helix is such that its wavelength is never shorter than 140 Å.

Acknowledgments

We are grateful to Bob Cubitt for lending us the D17 cryomagnet, S Raymond for help on setting up IN12, L Melesi and K Mony for technical assistance, M J Bull and P Manuel for help with preliminary measurements at ISIS, S M Hayden, S S Saxena, D Sheptyakov, F Bourdarot, J Schweizer, and C Pfleiderer for illuminating discussions, and Institut Laue-Langevin for providing beam time and partial coverage of travel expenses for RAS.

References

[1] Bak P and Jensen M H 1980 *J. Phys. C: Solid State Phys.* **13** L881
[2] Nakanishi O, Yanase A, Hasegawa A and Kataoka M 1980 *Solid State Commun.* **35** 995
[3] Plumer M L and Walker M B 1981 *J. Phys. C: Solid State Phys.* **14** 4689
[4] Kataoka M and Nakanishi O 1981 *J. Phys. Soc. Japan* **50** 3888
[5] Ishikawa Y, Tajima K, Bloch D and Roth M 1976 *Solid State Commun.* **19** 525
[6] Ishida M, Endoh Y, Mitsuda S, Ishikawa Y and Tanaka M 1985 *J. Phys. Soc. Japan* **54** 2975
[7] Shirane G *et al* 1983 *Phys. Rev.* B **28** 6251
[8] Okorokov A I *et al* 2004 *Physica* B **350** E323
[9] Thompson J D, Fisk Z and Lonzarich G G 1989 *Physica* B **161** 317
[10] Pfleiderer C, McMullan G J and Lonzarich G G 1994 *Physica* B **199/200** 634
[11] Thessieu C, Flouquet J, Lapertot G, Stepanov A N and Jaccard D 1995 *Solid State Commun.* **95** 707
[12] Pfleiderer C, McMullan G J and Lonzarich G G 1995 *Physica* B **206/207** 847
[13] Pfleiderer C, McMullan G J, Julian S R and Lonzarich G G 1997 *Phys. Rev.* B **55** 8330
[14] Pfleiderer C, Julian S R and Lonzarich G G 2001 *Nature* **414** 427
[15] Doiron-Leyraud N *et al* 2003 *Nature* **425** 595
[16] Pfleiderer C *et al* 2004 *Nature* **427** 227
[17] Moriya T 1985 *Spin Fluctuations in Itinerant Electron Magnetism* (Heidelberg: Springer)
Lonzarich G G and Taillefer L 1985 *J. Phys. C: Solid State Phys.* **18** 4339
[18] Thessieu C *et al* 1998 *J. Magn. Magn. Mater.* **177–181** 609
[19] Thessieu C, Kitaoka Y and Asayama K 1999 *Physica* B **259–261** 847

[20] Koyama K, Goto T, Kanomata T and Note R 2000 *Phys. Rev.* B **62** 986
[21] Yu W *et al* 2004 *Phys. Rev. Lett.* **92** 086403
[22] Gat-Malureanu I M *et al* 2003 *Phys. Rev. Lett.* **90** 157201
[23] Nakayama K and Moriya T 1987 *J. Phys. Soc. Japan* **56** 2918
[24] Roessli B, Böni P, Fischer W E and Endoh Y 2002 *Phys. Rev. Lett.* **88** 237204
[25] Ishikawa Y and Arai M 1984 *J. Phys. Soc. Japan* **53** 2726
[26] Belitz D, Kirkpatrick T R and Vojta T 1999 *Phys. Rev. Lett.* **82** 4707
[27] Vojta T and Sknepnek R 2001 *Phys. Rev.* B **64** 052404
[28] Rossat-Mignod J 1987 *Neutron Scattering* vol 23C *Methods of Experimental Physics* ed K Sköld and D L Price (New York: Academic) p 69